

Supporting Information

Pressure-Induced Room-Temperature Phosphorescence Enhancement Based on Purely Organic Molecules with Folding Geometry

Zhiqiang Yang,^{†a} Zhiyuan Fu,^{†b} Haichao Liu,^{*a} Min Wu,^b Nan Li,^b Kai Wang,^{*b} Shi-Tong Zhang,^a Bo Zou^{*b} and Bing Yang^{*a}

^a State Key Laboratory of Supramolecular Structure and Materials, College of Chemistry, Jilin University, Changchun 130012, China. E-mail: hcliu@jlu.edu.cn; yangbing@jlu.edu.cn

^b State Key Laboratory of Superhard Materials, College of Physics, Jilin University, Changchun 130012, China. E-mail: kaiwang@jlu.edu.cn; zoubo@jlu.edu.cn

† These authors contributed equally.

Content

S-I. General Information	S3
Structural characterization	S3
Single crystal X-ray diffraction (XRD) data	S3
Photophysical measurements	S3
Pressure-dependent experiment of crystal	S3
Theoretical calculation	S4
S-II. Synthetic details	S5
Scheme S1 Synthetic route to SeAN	S5
Synthesis of Selenanthrene (SeAN)	S5
S-III. SI Figures and tables	S6
Fig. S1 SOC constants at different folding angles	S6
Fig. S2 Photophysical properties of SeAN and TA in dilute solution	S7
Fig. S3 Configurations and spectra of SeAN and TA in their crystals	S8
Fig. S4 Absorption experiments of SeAN crystals under high pressure.....	S9
Fig. S5 Emission experiments of SeAN crystal above 4.15 GPa	S10
Fig. S6 Emission experiments of SeAN crystal during depressurization	S10
Fig. S7 High-pressure angle dispersive XRD patterns for SeAN crystals.....	S11
Fig. S8 Crystal characteristics of SeAN under high pressure	S11
Fig. S9 Hirshfeld surface analysis for SeAN monomers	S12
Fig. S10 Relative contributions of intermolecular contacts	S13
Fig. S11 Energy levels of the SeAN monomer	S14
Fig. S12 Comparison of SOC constants at different pressures	S14
Fig. S13 Estimation of parameters related to the RTP radiation process	S15
Fig. S14 Pressure-dependent lifetime of SeAN crystals	S16
Table S1 Parameters of pressure- dependent PLQY	S17
Fig. S15 Electronic transition analysis in SeAN dimer	S18
Fig. S16 SOC coefficients of SeAN dimer as a function of external pressure	S19
Fig. S17 The relationship between folding angle and transition behaviour.....	S20
Fig. S18 Composition of emission spectra of TA at different pressures	S21
Fig. S19 ¹ H NMR spectrum of SeAN compound	S22
Fig. S20 ¹³ C NMR spectrum of SeAN compound	S22
S-IV. References	S23

S-I. General Information

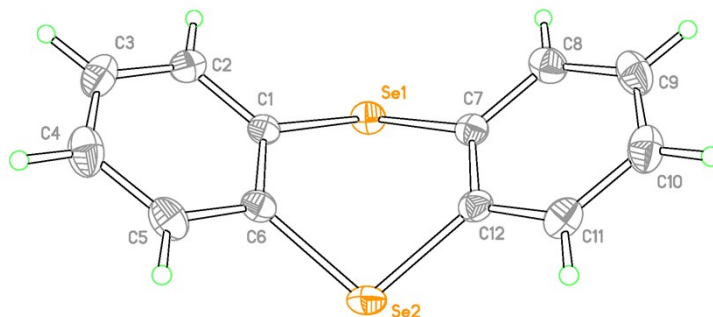
Structural characterization: All the reagents and solvents used for the synthesis and experiments were purchased from J&K Scientific companies and used without further purification. ^1H and ^{13}C NMR spectra were recorded on a Bruker AVANCE 500 spectrometer, using tetramethylsilane (TMS) as the internal standard. The mass spectra (MS) were recorded using an ITQ1100 (Thermo Fisher).

Single crystal X-ray diffraction (XRD) data: Single crystals of SeAN were grown by sublimation. The diffraction experiments were carried out on a Rigaku R-Axis RAPID diffractometer equipped with a Mo-K α and control Software using the RAPID AUTO. The crystal structures were solved with direct methods and refined with a full-matrix least-squares technique using the Olex2 programs.

Crystallographic information:

TA from Cambridge Structural Database, CCDC number: 1836801.

SeAN (CCDC number: 2213389): crystal color: colorless, empirical formula: $\text{C}_{12}\text{H}_8\text{Se}_2$, formula weight: 310.10, $T = 288\text{K}$, crystal system: monoclinic; space group: P 2 $1/c$; $a = 12.1157 \text{ \AA}$, $b = 6.2539 \text{ \AA}$, $c = 14.6000 \text{ \AA}$, $\alpha = 90^\circ$, $\beta = 109.833^\circ$, $\gamma = 90^\circ$, $V = 1040.63 \text{ \AA}^3$, $Z = 4$, $F(000) = 592.0$, density = 1.979g/cm^3 , $\mu = 7.058 \text{ mm}^{-1}$; reflections collected: 17856; unique reflections: 2206; $R(\text{int}) = 0.0395$, $\text{GOF} = 1.052$, $R_1 [I > 2\sigma(I)] = 0.0203$, $\omega R_2 [I > 2\sigma(I)] = 0.0456$, $R_1(\text{all data}) = 0.0253$, $\omega R_2(\text{all data}) = 0.0473$.



Photophysical measurements: UV-vis spectra of solutions were recorded on a PerkinElmer Lambda 365 Spectrophotometer. Steady-state emission spectra and lifetimes were collected on an Edinburgh Instruments FLS980 Spectrometer. Photoluminescence quantum yields (PLQYs) were measured using an integrating sphere apparatus. Solutions were placed in 1 cm path length quartz cells and crystals were fixed on quartz plate in terms of steady-state emission spectra and lifetimes.

Pressure-dependent experiment of crystal: A symmetric diamond anvil cell (DAC) with 400 μm diameter culet diamonds was used in high-pressure RTP, absorption, and synchrotron XRD experiments. A T301 steel gasket with a 150 μm diameter and

thickness 45 μm hole in the center was placed in DAC. Crystals were loaded in the gasket hole together with a small ruby ball to measure the pressure by using a standard ruby-fluorescence method. For the single crystal of SeAN studied under high pressure, silicone oil was used as the pressure-transmitting medium (PTM). All of the high-pressure experiments were conducted at room temperature.

In situ photoluminescence measurements under high pressure were performed on an Ocean Optics QE65000 spectrometer. A 355 nm line of UV DPSS laser with a spot size of 40 μm was used.

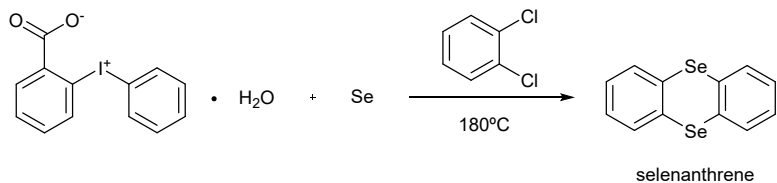
In situ high-pressure absorption spectra were recorded by an optical fiber spectrometer (Ocean Optics, QE65000). The real optical photographs were obtained by using a Canon EOS 5D camera equipped with a reflection lens.

In situ high-pressure angle-dispersive XRD (ADXRD) experiments were conducted on the BL15U1 beamline of Shanghai Synchrotron Radiation Facility (SSRF). Monochromatic beam wavelength used for data collection was 0.6199 \AA with a $2 \times 3 \mu\text{m}^2$ size. The distance of the sample detector and the geometric parameters were calibrated by a CeO_2 standard. Dioptas software was utilized to yield plots of intensity versus 2θ as recorded two-dimensional (2D) data.

Theoretical calculation: Density functional theory (DFT) was carried out for the ground-state geometry optimization at the level of CAM-B3LYP/6-31G(d, p) using Gaussian 09 (version D.01) package^[1] on a Power Leader cluster. Time-dependent density functional theory (TD-DFT) was carried out for natural transition orbitals (NTOs) at the level of CAM-B3LYP/6-31G(d, p). Spin-orbit coupling (SOC) coefficients were quantitatively estimated at the level of CAM-B3LYP/6-31G(d, p) by Beijing density function (BDF)^[2-8] program. Transition density matrix (TDM) maps of dimer were obtained by Multiwfn Software.^[9] Using the unit cell parameters under different pressures measured by in situ high pressure ADXRD experiments, geometry optimization was performed for the SeAN under different pressures, based on the first principles plane-wave pseudopotential DFT^[10] as implemented in the CASTEP package^[11]. The GGA functional of Perdew, Burke, and Ernzerhof^[12] was used in the calculation. To correct the van der Waals interactions common in molecular crystals, nonempirical scheme of the TS^[13] was used. The convergence levels for total energy, max force, max stress, max displacement, and SCF iterations were ultra-fine. In order to visualize and analyze the intermolecular interactions in the crystal structures of SeAN under different pressures, a Crystal Explorer 21.5 program^[14] was used. It enabled us to construct the three-dimensional (3D) Hirshfeld surfaces of molecules in crystals.^[15] We also could get information about relative contributions of intermolecular contacts to the Hirshfeld surface area from it.^[16]

S-II. Synthetic details

TA and diphenyliodonium-2-carboxylate monohydrate sample was purchased from J&K Scientific. TA was further purified by sublimation method and diphenyliodonium-2-carboxylate monohydrate was used directly without purification.



Scheme S1 | Synthetic route to SeAN.

Synthesis of Selenanthrene (SeAN)

Synthesis of SeAN is accomplished in one step. Add **Se powder (789 mg, 10mmol)** and **diphenyliodonium-2-carboxylate monohydrate (1.72 g, 5 mmol)** to **1,2-dichlorobenzene (50 mL)**. The mixture was heated to 180°C and stirred for 3 hours. The mixture was cooled to room temperature and the solvent was removed by flash silica gel column chromatography by petroleum ether to obtain a tan crude product. The crude product was purified by sublimation to obtain 300 mg of colorless and transparent crystals with a yield of ~19%. ¹H NMR (500 MHz, DMSO-*d*₆, 25 °C, TMS): δ 7.79 (dd, J = 5.7, 3.4 Hz, 4H, Ar-H), 7.35 (dd, J = 5.8, 3.4 Hz, 4H, Ar-H); ¹³C NMR (125 MHz, CDCl₃, 25 °C, TMS): δ = 134.53 (C), 131.22 (CH), 128.08 (CH); GC-MS, EI, mass m/z: 312.03 [M⁺].

S-III. SI Figures and tables

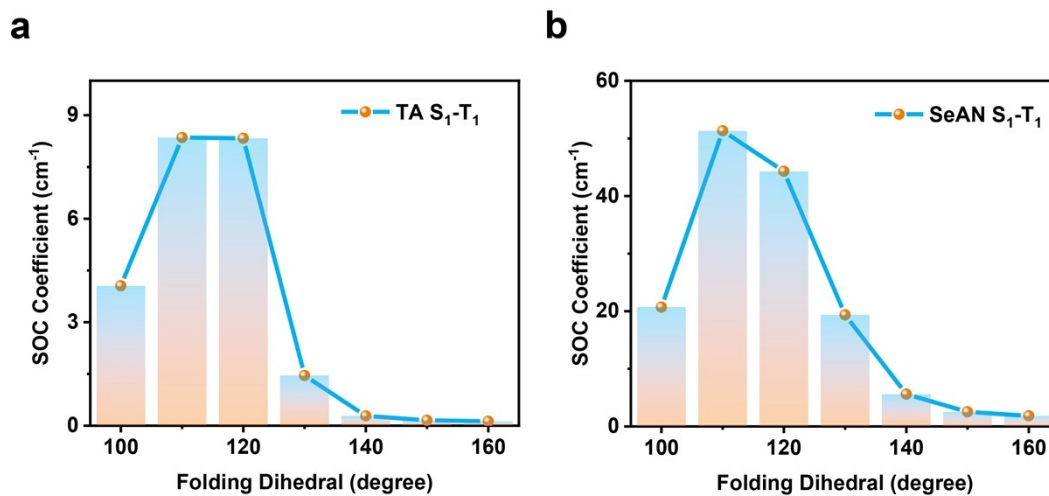


Fig. S1 | SOC coefficient between S_1 and T_1 as a function of folding dihedral angle for (a) TA and (b) SeAN.

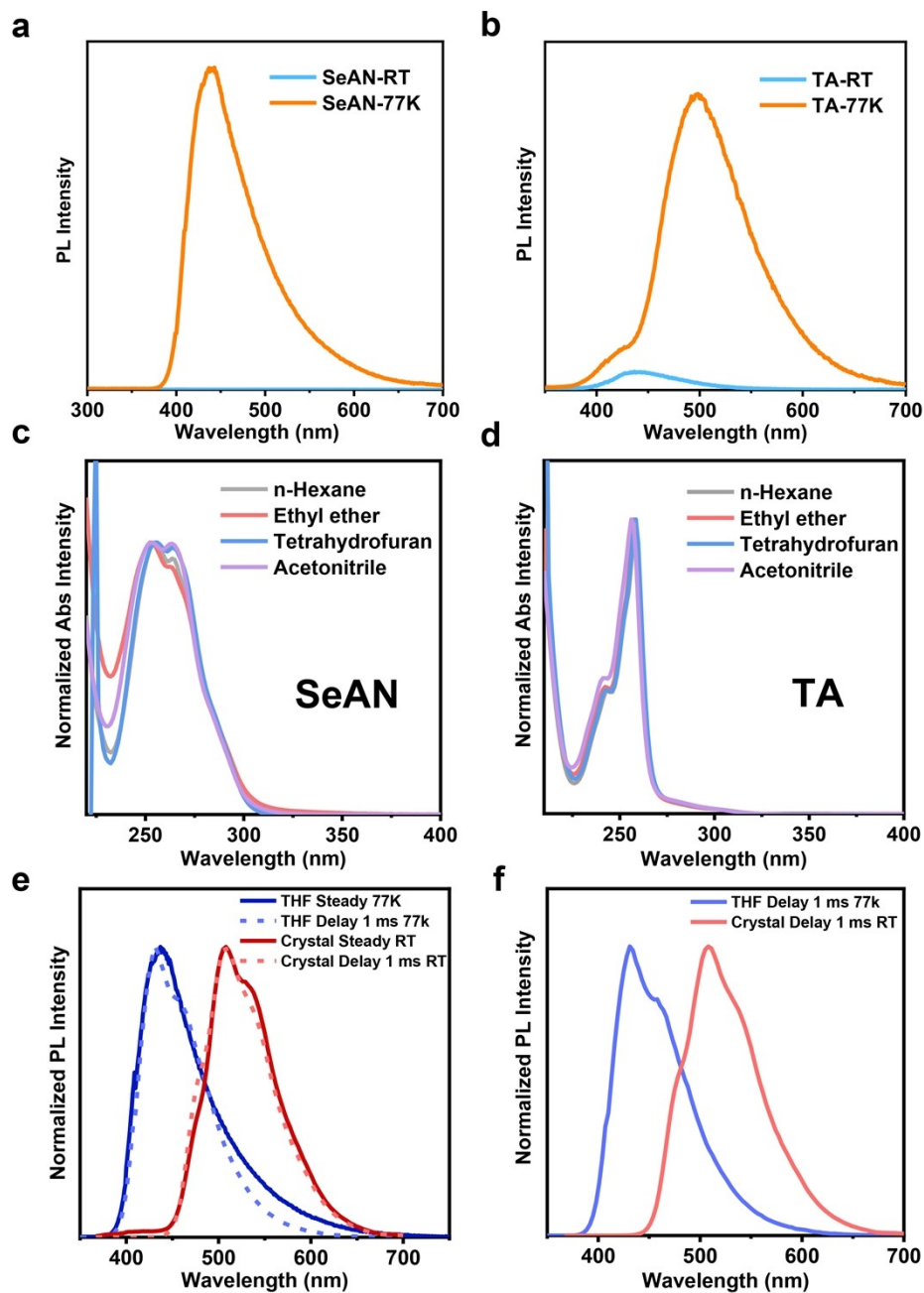


Fig. S2 | Emission spectrum of **(a)** SeAN in tetrahydrofuran (THF, 10^{-5} M) and **(b)** TA in tetrahydrofuran (10^{-5} M) at room temperature (RT) and 77 K. Absorption spectra of **(c)** SeAN and **(d)** TA in different solvents. **(e)** Steady and delayed emission spectra of SeAN in tetrahydrofuran (10^{-5} M, 77 K) and crystal (RT). **(f)** Delayed emission spectra of SeAN in tetrahydrofuran (10^{-5} M, 77 K) and crystal (RT).

SeAN shows a vibronic-structured emission spectrum after a delay of 1 ms, corresponding to a phosphorescence emission from locally excited triplet state.

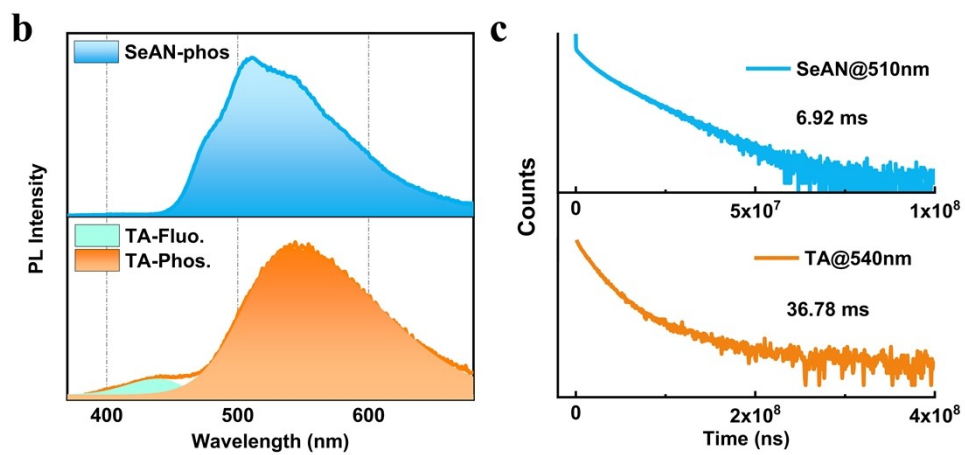
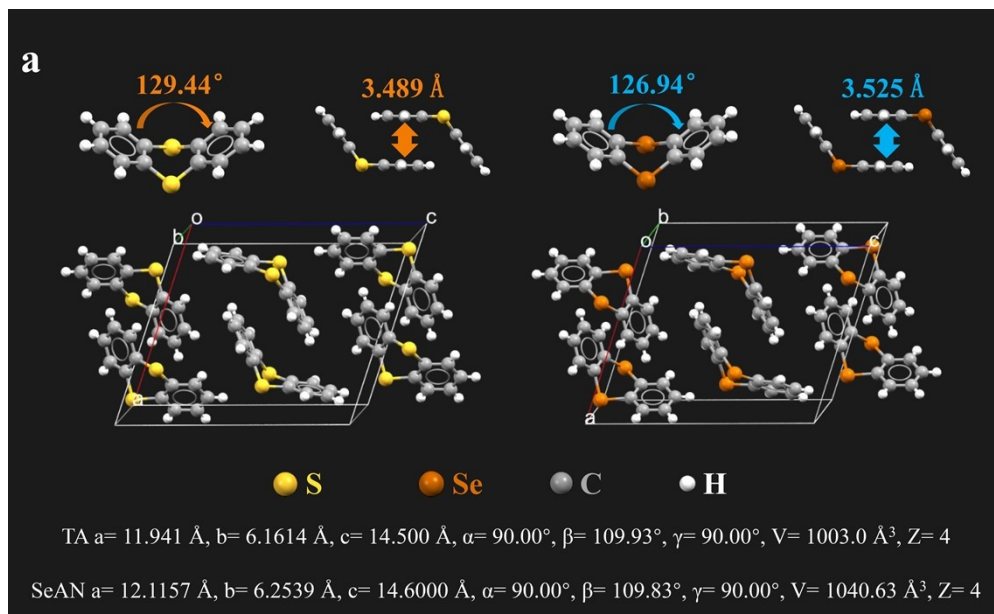
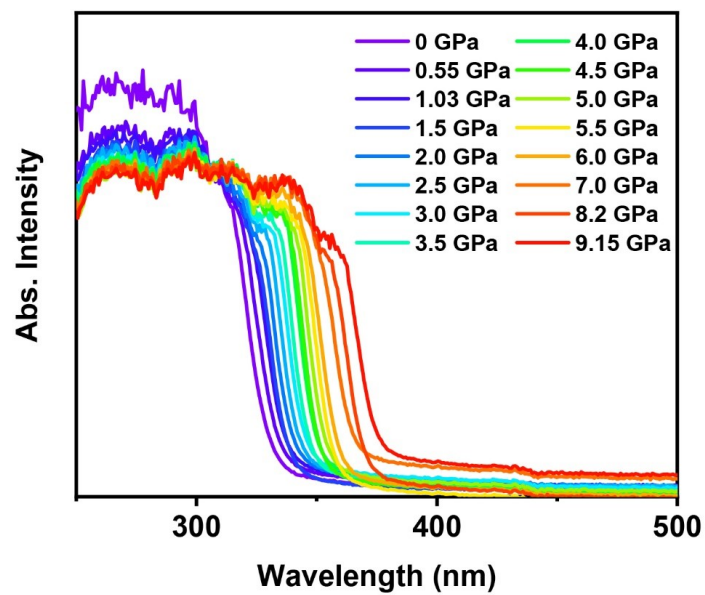


Fig. S3 | **(a)** Comparison of geometry and packing motif of SeAN and TA in crystals. **(b)** Steady emission spectra and **(c)** time-resolved emission spectra of SeAN and TA crystals

a



b

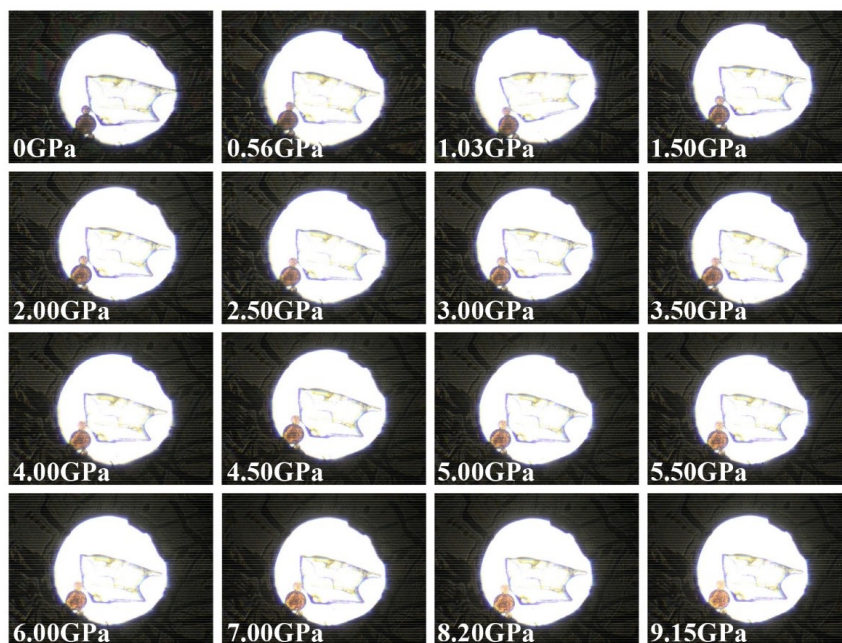


Fig. S4 | (a) Absorption spectra and (b) photographs of SeAN crystals under different pressures.

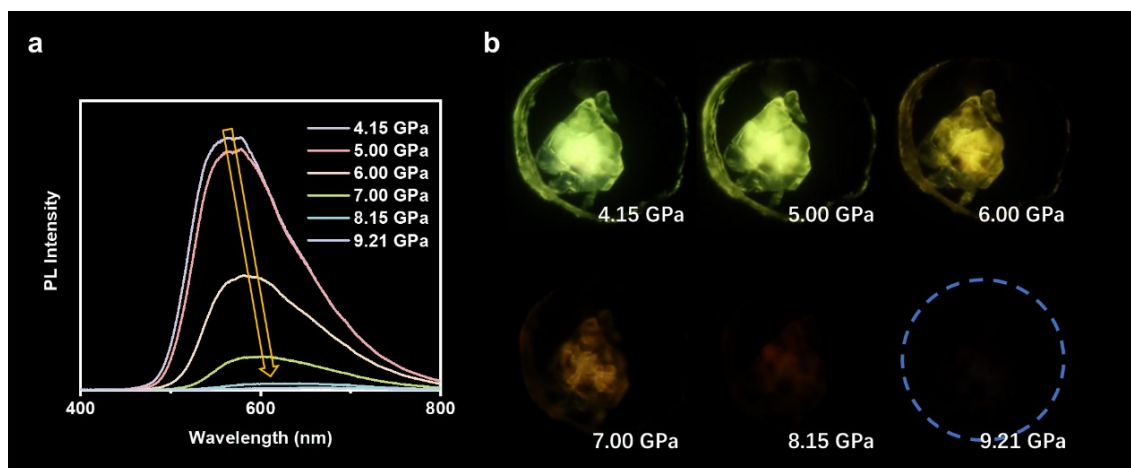


Fig. S5 | (a) Emission spectra and (b) luminescence photographs of SeAN crystals under different pressures (4.15-9.21 GPa).

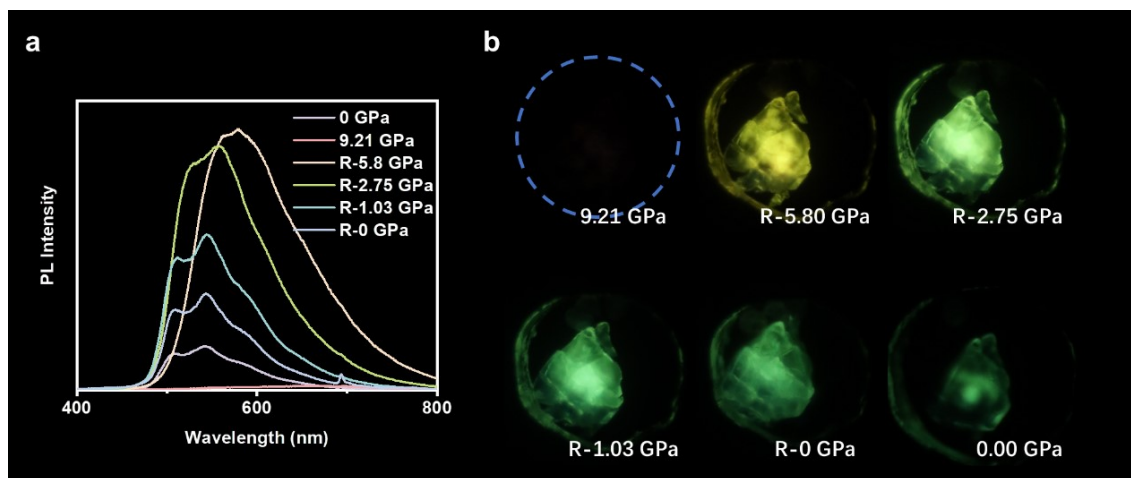


Fig. S6 | (a) Emission spectra and (b) luminescence photographs of SeAN crystals during decompression.

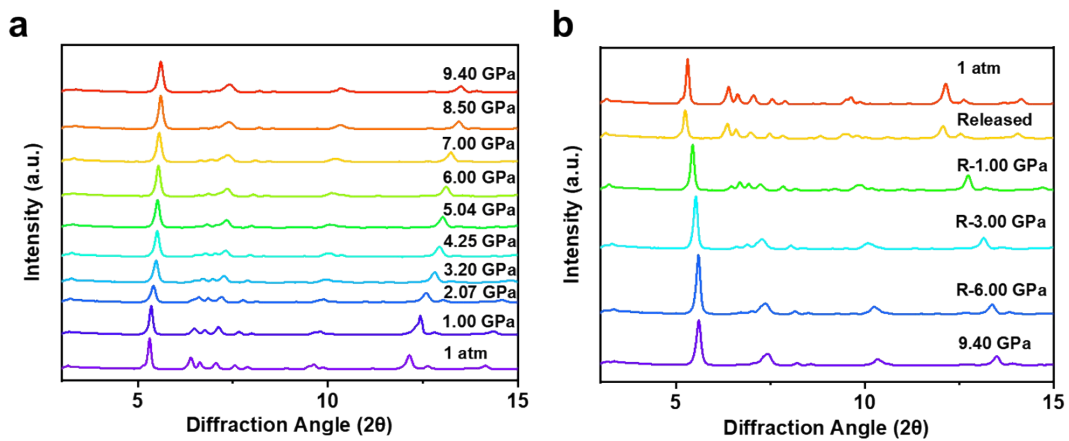


Fig. S7 | High-pressure ADXRD for SeAN crystals during (a) pressurization and (b) decompression.

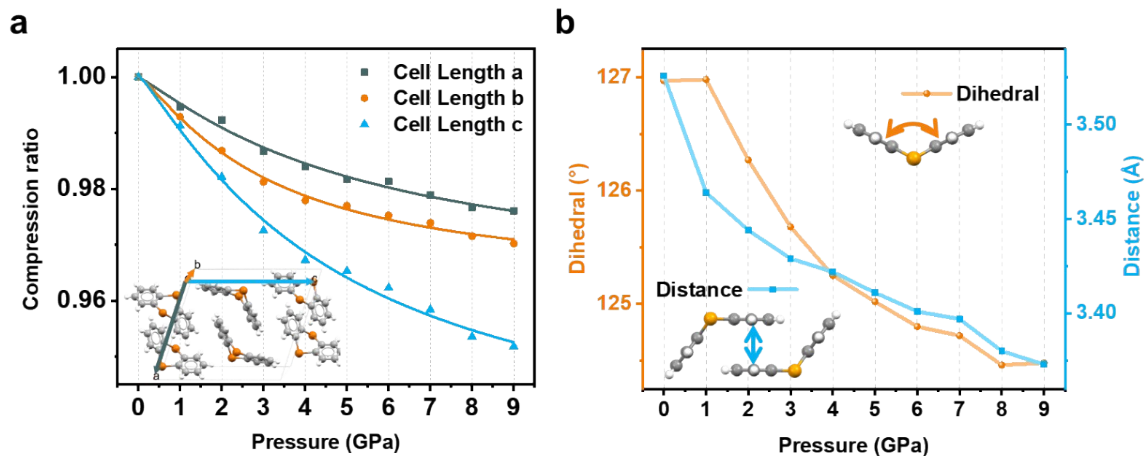


Fig. S8 | (a) Crystal axis parameters and (b) molecular folding angle and π - π distance for SeAN crystal under different pressures.

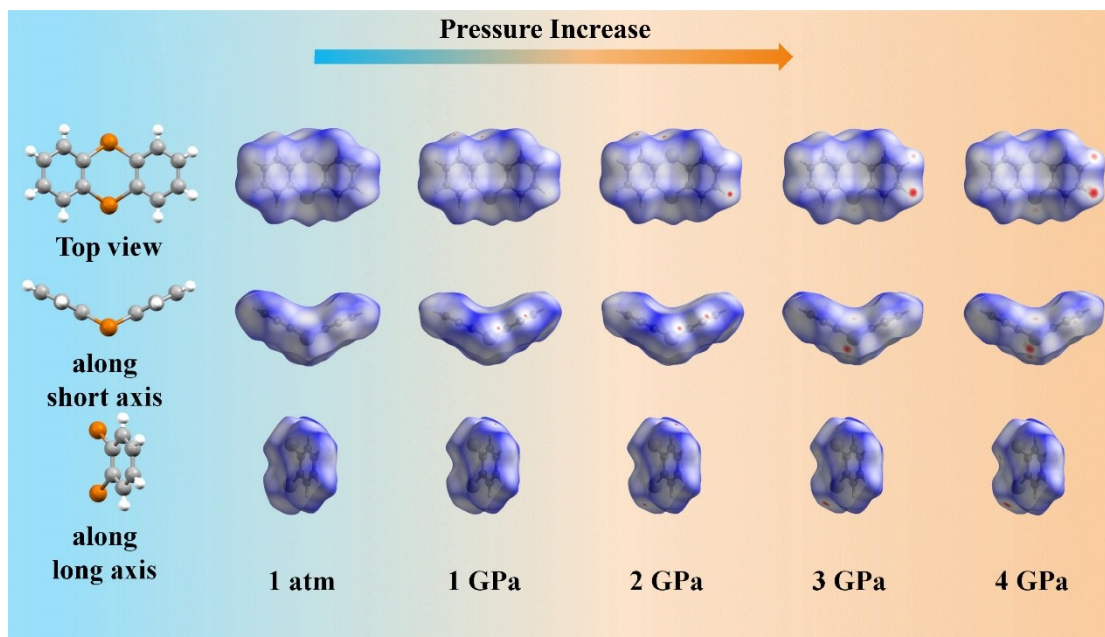


Fig. S9 | Hirshfeld surface analysis for monomers in SeAN crystals under different pressures.

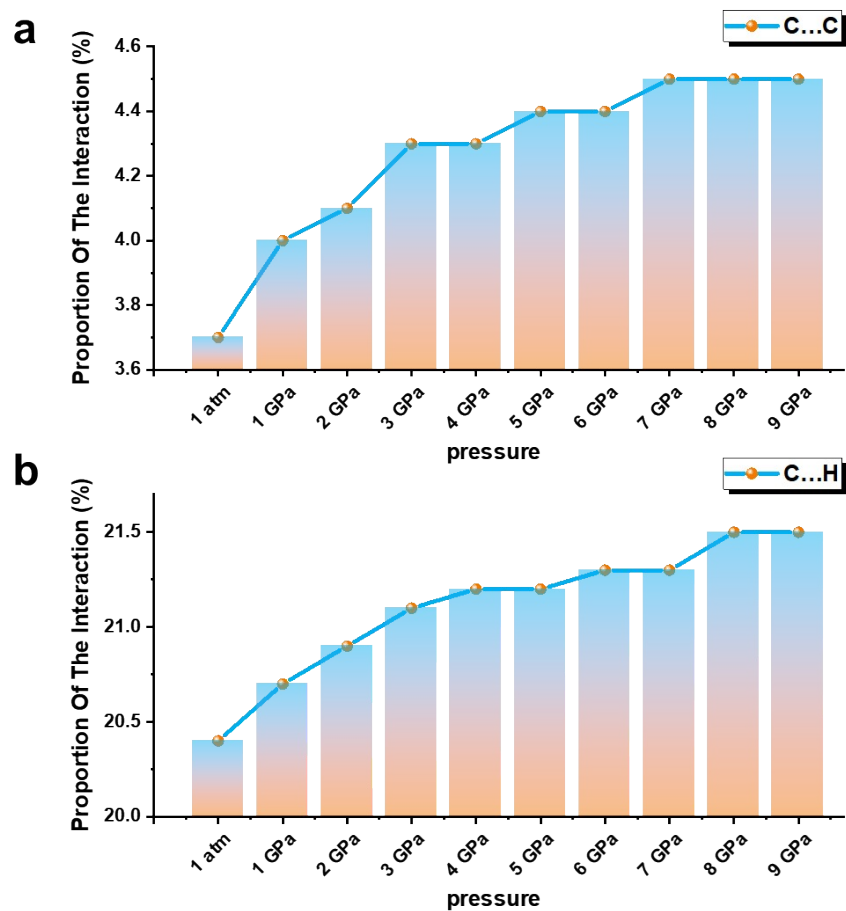


Fig. S10 | Proportion of the (a) C...C and (b) C...H interactions under different pressures.

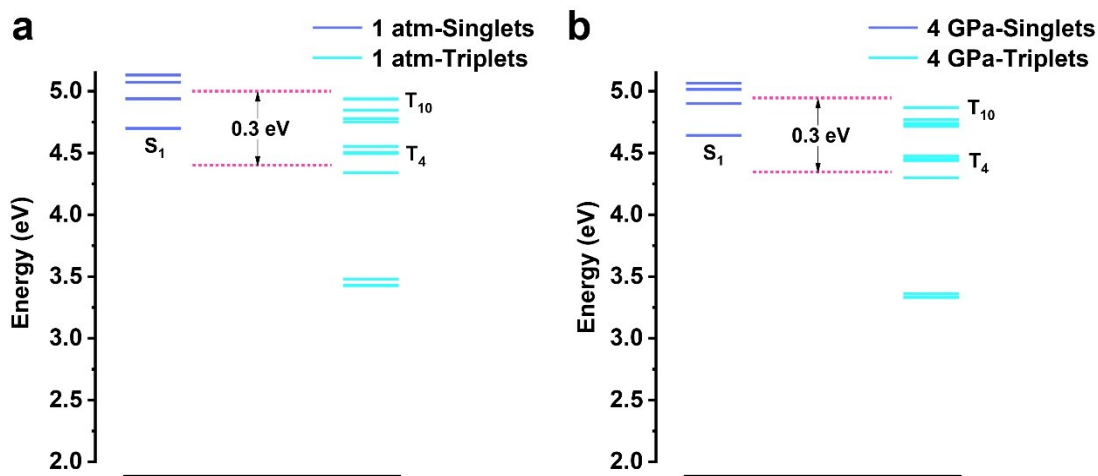


Fig. S11 | Energy levels of the SeAN monomer at (a) 1 atm and (b) 4 GPa.

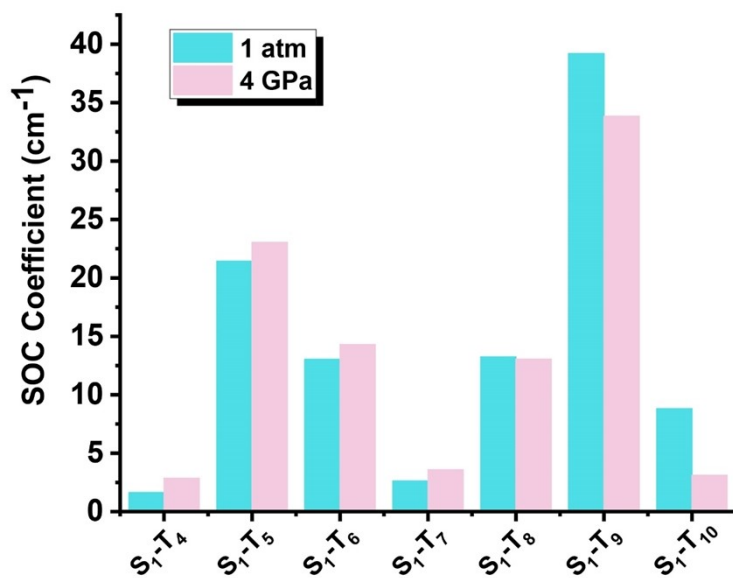


Fig. S12 | Comparison of SOC coefficients of SeAN monomer between different singlet and triplet states (T₄-T₁₀) at 1 atm and 4 GPa.

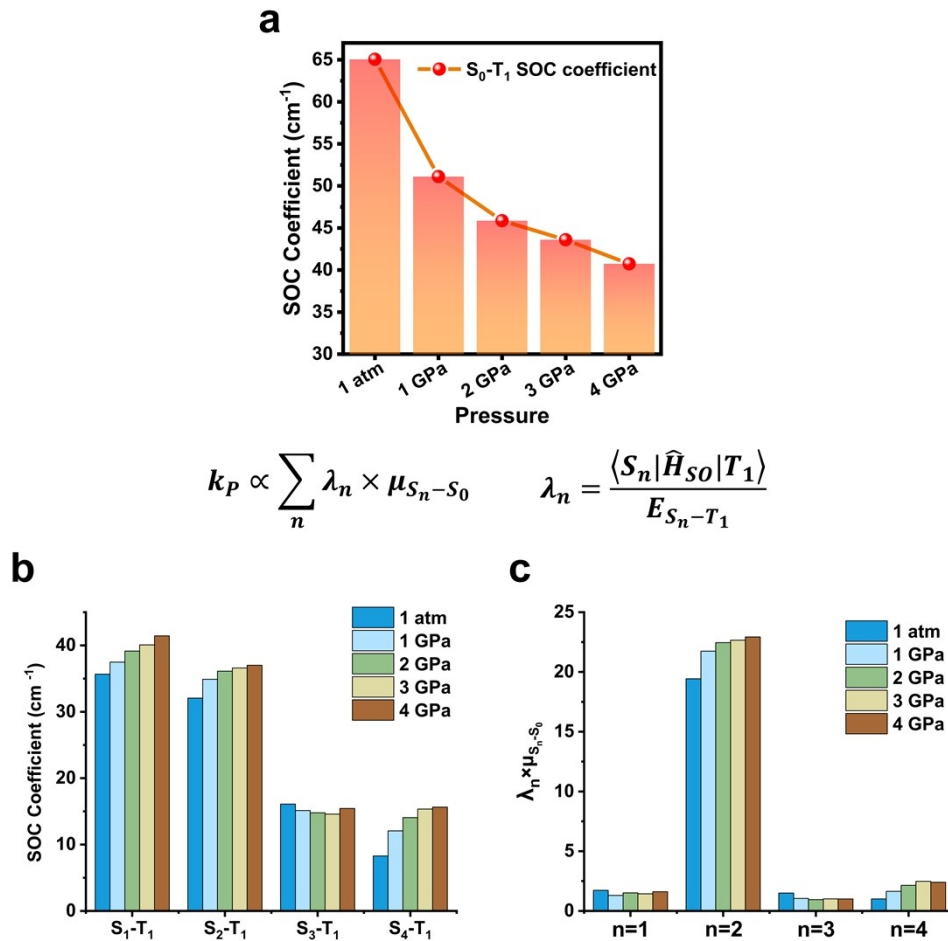


Fig. S13 | (a) SOC coefficients between S_0 - T_1 of SeAN monomer under different pressures. (b) Comparison of SOC coefficients of SeAN monomer between different singlets (S_1 - S_4) and the lowest triplet state (T_1) under different pressures. (c) Estimation of parameters related to k_p (phosphorescence radiation rate).

SOC coefficient between T_1 and S_0 gradually decreases with an increase in external pressure. According to photophysical understanding of RTP, [17-18] a decreased SOC between T_1 and S_0 facilitates to suppress the non-radiative transition process (i.e. the ISC process from T_1 to S_0). On the other hand, the intensity-borrowing strategy is also used to understand the enhanced RTP radiation from the forbidden transition of $T_1 \rightarrow S_0$ through the state mixing mechanism between T_1 and S_n . [19-23] With growing pressure, most of SOC coefficients between T_1 and S_n are also increased, in favor of the more singlet component mixed into T_1 state, resulting in the RTP enhancement under high pressure by accelerating the radiative process to some extent.

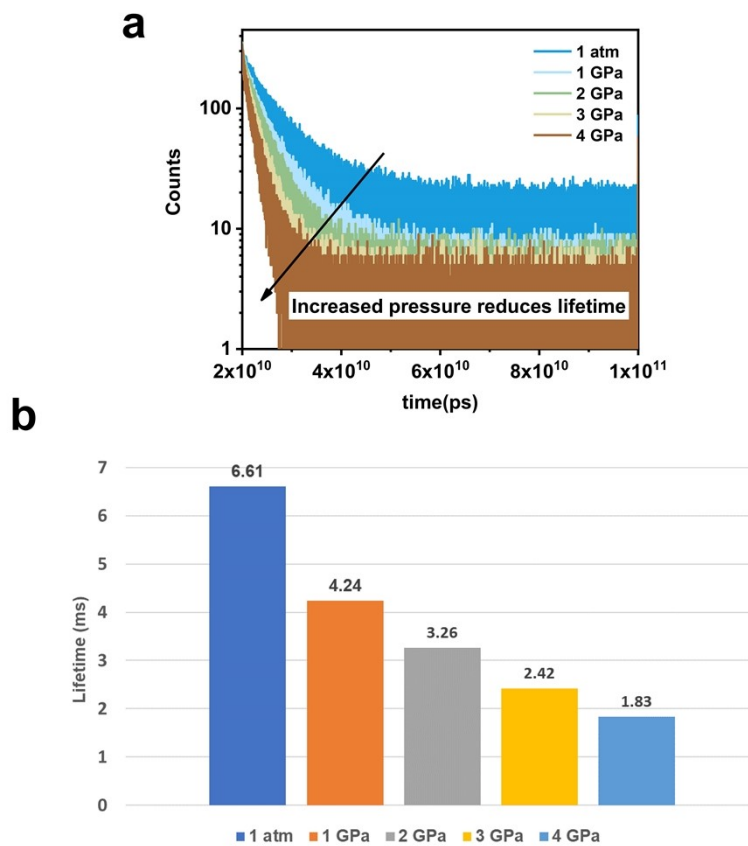


Fig. S14 | Pressure-dependent (a) time-resolved emission spectra and (b) average lifetimes of SeAN crystals.

Table S1 | Parameters of pressure- dependent PLQY.

Pressure (GPa)	PL integral intensity I/I_0	Cell volume V/V_0	Average lifetime (ms)	Absorbance A_0/A	Φ'
ambient pressure	1	1	6.61	1	4.80 %
1	4.07	0.98	4.24	0.67	13.09 %
2	6.99	0.96	3.26	0.63	21.24 %
3	10.05	0.94	2.42	0.55	26.53 %
4	12.86	0.93	1.83	0.49	30.25 %

It is challenging to measure the RTP radiation ability of SeAN crystal under different pressures. However, the PLQY under different pressures can be estimated by the following formula: [24-25]

$$\begin{aligned}
\Phi &= \Phi_0 \frac{\int F(\lambda_{em})}{\int F_0(\lambda_{em})} \cdot \frac{A_0(\lambda_{ex})}{A(\lambda_{ex})} \cdot \frac{n^2}{n_0^2} \\
&= \Phi_0 \frac{I}{I_0} \cdot \frac{A_0}{A} \cdot \frac{n^2}{n_0^2} \\
&= \Phi' \cdot \frac{n^2}{n_0^2}
\end{aligned} \tag{1}$$

where Φ is the PLQY of SeAN crystal under different pressures, $\int F(\lambda_{em})$ is the integrated intensity of emission, $A(\lambda_{ex})$ is the percentage of light absorbed at excitation wavelength, n is the refractive index, and the subscript 0 denotes the reference data under ambient pressure.

The correction factor (n^2/n_0^2) can be calculated from the cell volume under pressure by the Clausius-Mossotti equation and the Lorentz-Lorenz equation: [26-27]

$$\frac{n^2 - 1}{n^2 + 2} \cdot \frac{1}{\rho} = \frac{4\pi}{3} \cdot N_A \cdot \alpha = R_{LL} \tag{2}$$

The density ρ can be calculated from the cell volume obtained by ADXRD. R_{LL} is called the Lorentz-Lorenz constant, and R_{LL} is related to the polarizability α . It can be inferred that as the pressure increases, the cell volume decreases and the density ρ increases, and the corresponding n^2 also increases. Therefore, the correction factor at high pressure is greater than 1, making the actual pressure-dependent PLQY(Φ) larger than Φ' .

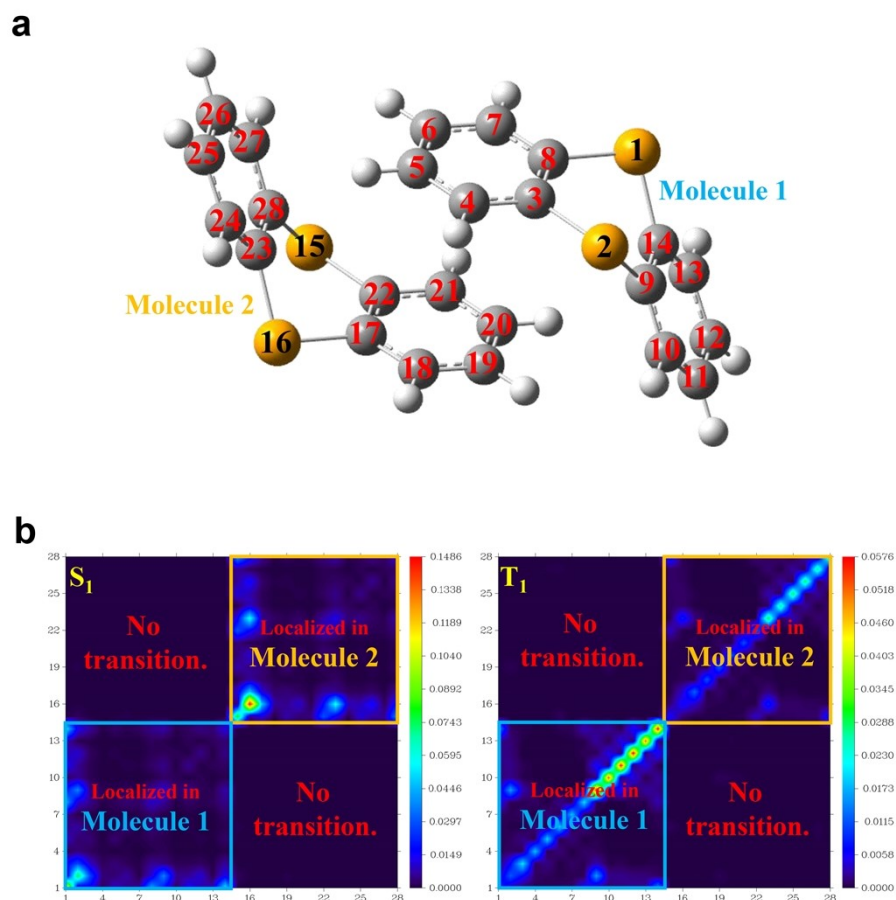


Fig. S15 | (a) Atoms were numbered before transition density analysis. (b) Transition density heatmaps for S_1 and T_1 states based on the molecular configuration at 4 GPa.

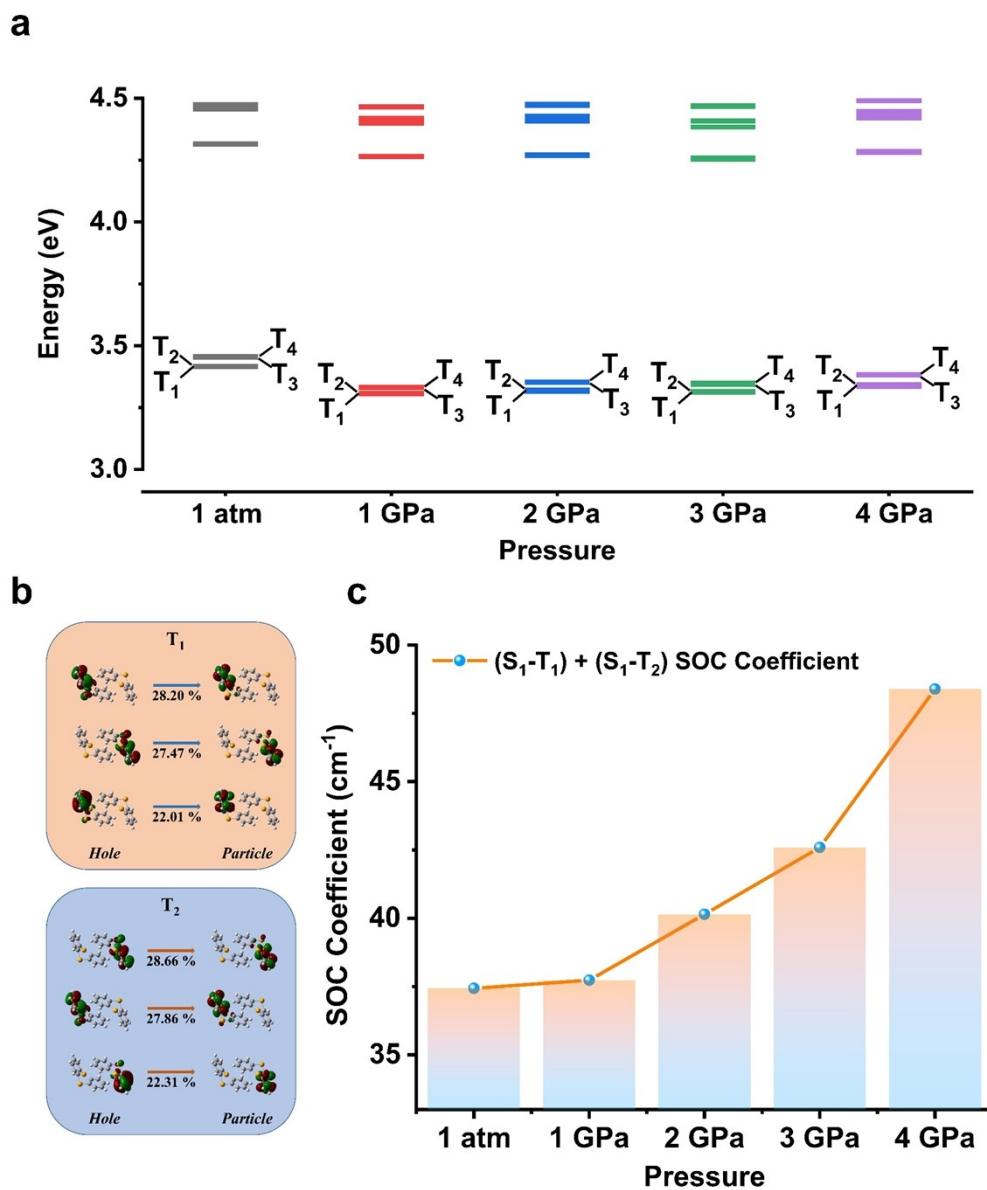


Fig. S16 | (a) Triplet energy levels of SeAN dimer under different pressures and (b) NTOs of the T_1 and T_2 states of SeAN dimer at 1 atm. (c) The sum of the SOC coefficients of S_1-T_1 and S_1-T_2 of SeAN dimer under different pressures.

It can be seen that the T_1 and T_2 states are actually degenerated. Therefore, the sum of the SOC coefficients of S_1-T_1 and S_1-T_2 of SeAN dimer is more meaningful.

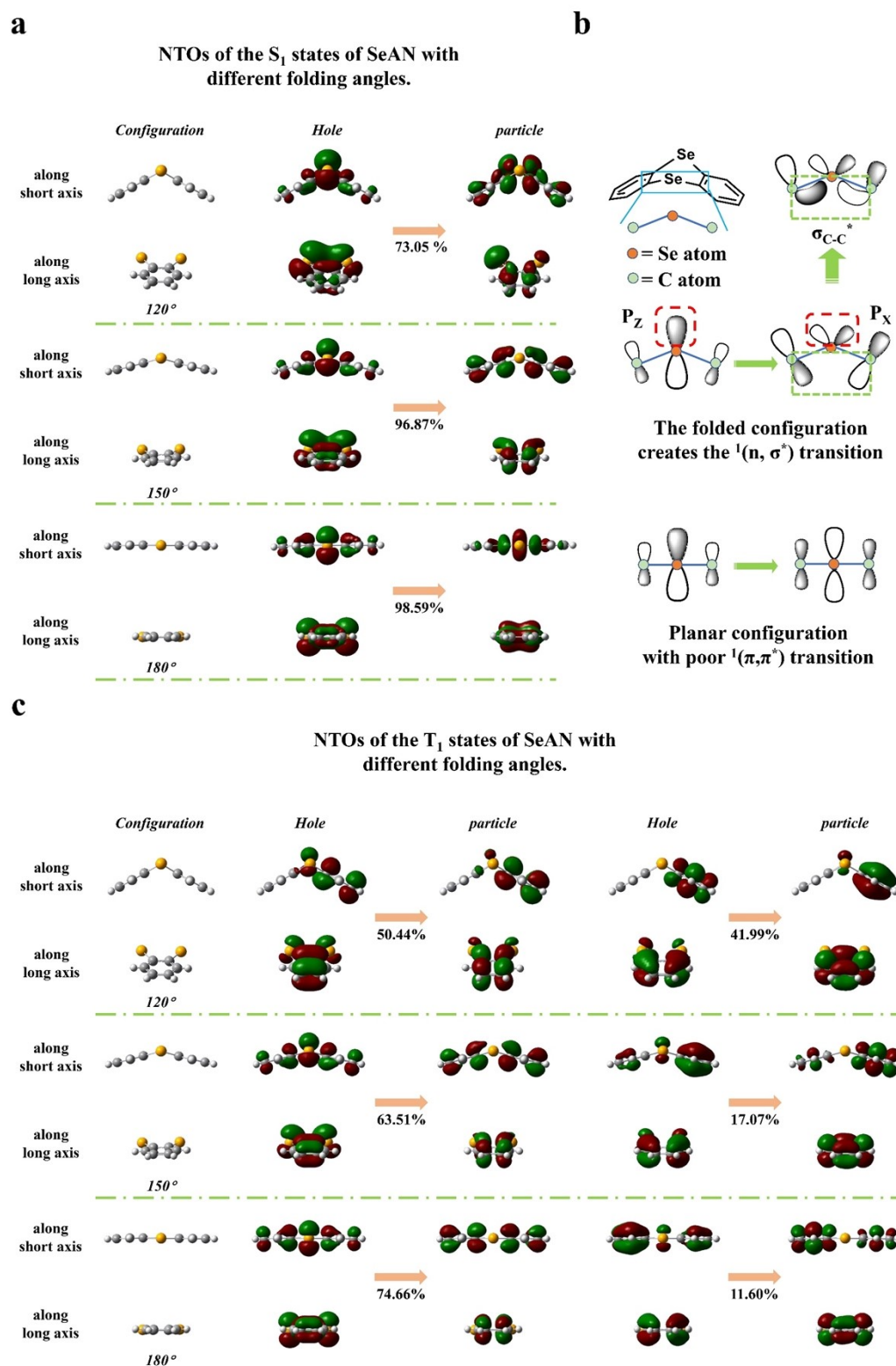


Fig. S17 | (a) NTOs of the S_1 states of SeAN with different folding angles. (b) The relationship between folding angle and transition configuration. (c) NTOs of the T_1 states of SeAN with different folding angles.

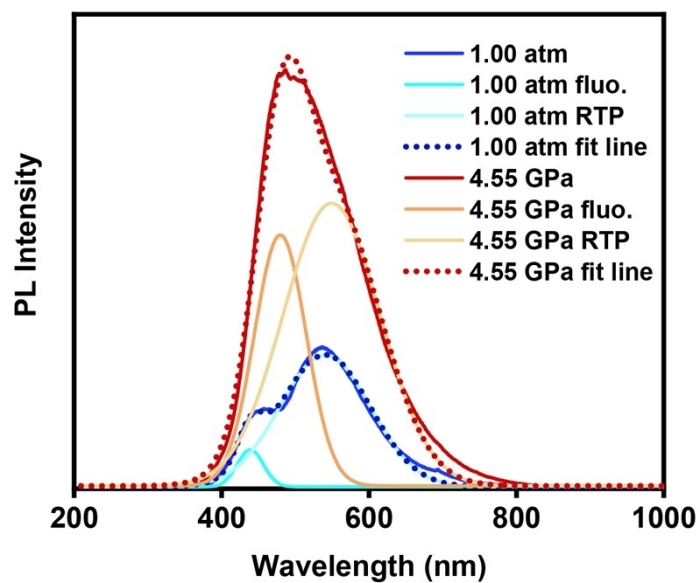


Fig. S18 | Composition of emission spectra of TA crystals under different pressures.

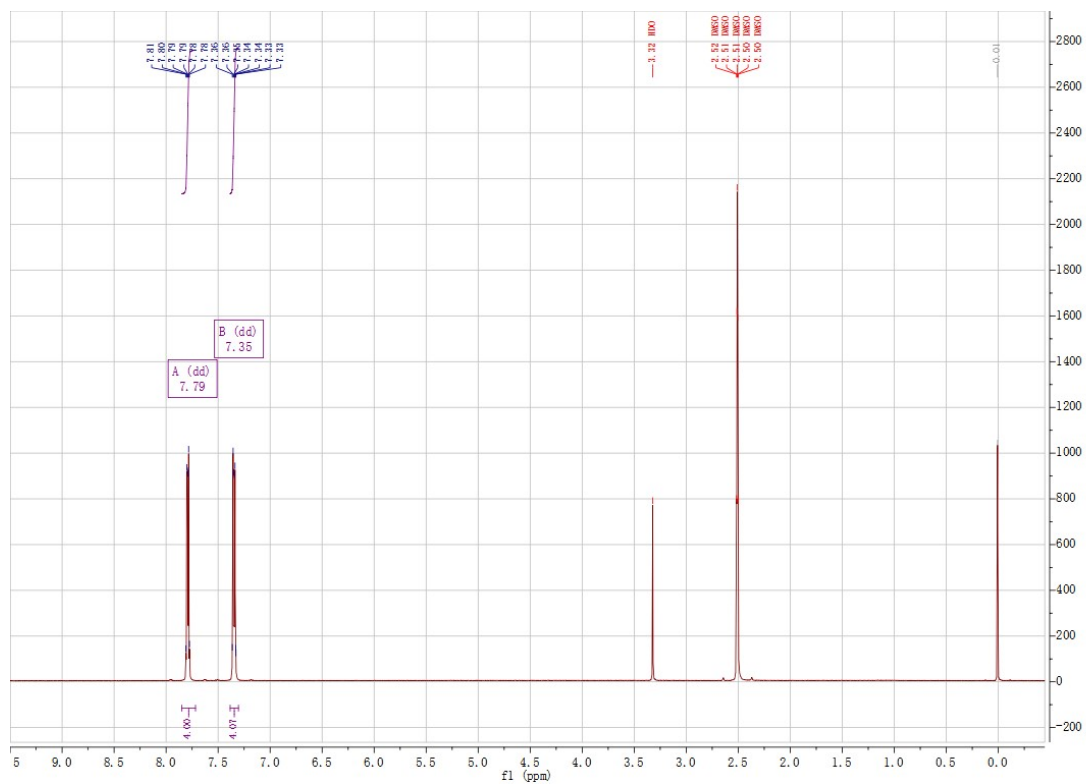


Fig. S19 | ¹H NMR spectrum of SeAN compound.

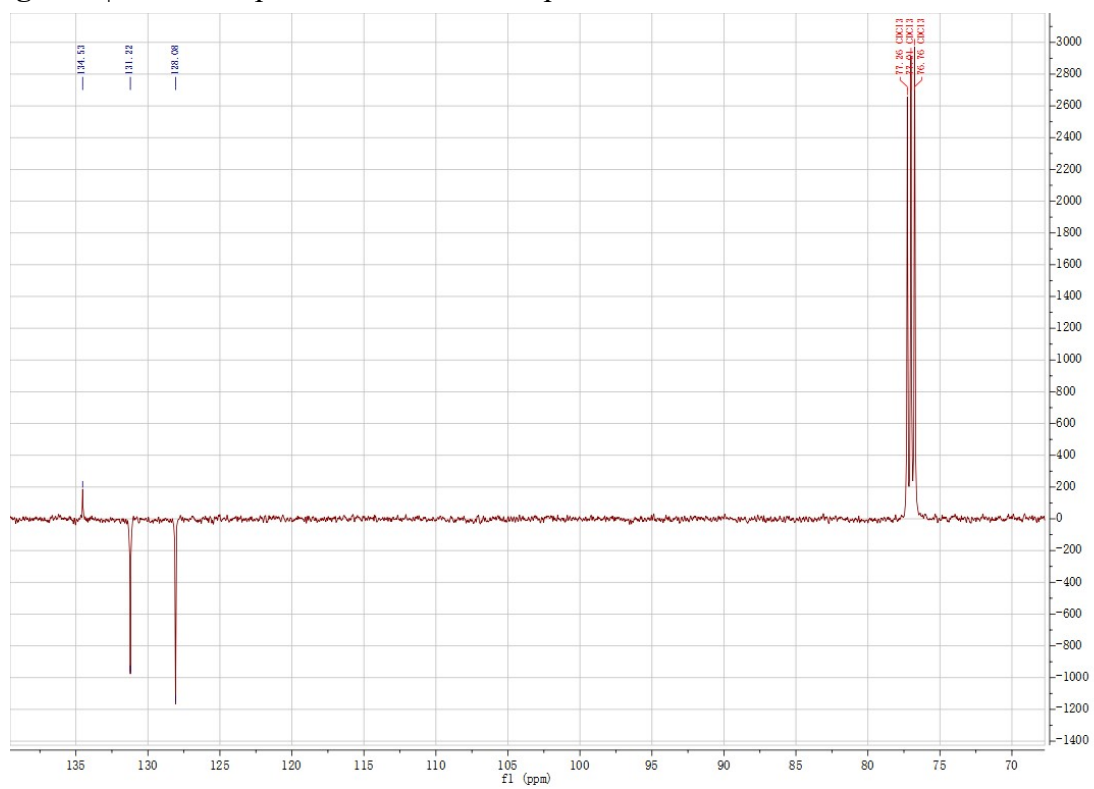


Fig. S20 | ¹³C NMR spectrum of SeAN compound.

S-IV. References

- [1] Frisch, M. J.; Trucks, G. W.; Schlegel, H. B.; Scuseria, G. E.; Robb, M. A.; Cheeseman, J. R.; Scalmani, G.; Barone, V.; Mennucci, B.; Petersson, G. A.; Nakatsuji, H.; Caricato, M.; Li, X.; Hratchian, H. P.; Izmaylov, A. F.; Bloino, J.; Zheng, G.; Sonnenberg, J. L.; Hada, M.; Ehara, M.; Toyota, K.; Fukuda, R.; Hasegawa, J.; Ishida, M.; Nakajima, T.; Honda, Y.; Kitao, O.; Nakai, H.; Vreven, T.; Montgomery, J. A.; Jr.; Peralta, J. E.; Ogliaro, F.; Bearpark, M.; Heyd, J. J.; Brothers, E.; Kudin, K. N.; Staroverov, V. N.; Keith, T.; Kobayashi, R.; Normand, J.; Raghavachari, K.; Rendell, A.; Burant, J. C.; Iyengar, S. S.; Tomasi, J.; Cossi, M.; Rega, N.; Millam, J. M.; Klene, M.; Knox, J. E.; Cross, J. B.; Bakken, V.; Adamo, C.; Jaramillo, J.; Gomperts, R.; Stratmann, R. E.; Yazyev, O.; Austin, A. J.; Cammi, R.; Pomelli, C.; Ochterski, J. W.; Martin, R. L.; Morokuma, K.; Zakrzewski, V. G.; Voth, G. A.; Salvador, P.; Dannenberg, J. J.; Dapprich, S.; Daniels, A. D.; Farkas, Ö.; Foresman, J. B.; Ortiz, J. V.; Cioslowski, J.; Fox, D. J. Gaussian 09, Revision D.01; Gaussian, Inc., Wallingford CT, 2013.
- [2] Liu, W.; Hong, G.; Dai, D.; Li, L.; Dolg, M. The Beijing four-component density functional program package (BDF) and its application to EuO, EuS, YbO and YbS. *Theor. Chem. Acc.* 1997, **96**, 75-83.
- [3] Zhang, Y.; Suo, B.; Wang, Z.; Zhang, N.; Li, Z.; Lei, Y.; Zou, W.; Gao, J.; Peng, D.; Pu, Z.; et al. BDF: A relativistic electronic structure program package. *J. Chem. Phys.* 2020, **152**, 064113.
- [4] Liu, W.; Wang, F.; Li, L. The Beijing Density Functional (BDF) Program Package: Methodologies and Applications. *J. Theor. Comput. Chem.* 2003, **02**, 257-272.
- [5] Liu, W.; Wang, F.; Li, L. RELATIVISTIC DENSITY FUNCTIONAL THEORY: THE BDF PROGRAM PACKAGE. In *Recent Advances in Relativistic Molecular Theory*, pp 257-282.
- [6] Li, Z.; Suo, B.; Zhang, Y.; Xiao, Y.; Liu, W. Combining spin-adapted open-shell TD-DFT with spin-orbit coupling. *Mol. Phys.* 2013, **111**, 3741-3755.
- [7] Li, Z.; Xiao, Y.; Liu, W. On the spin separation of algebraic two-component relativistic Hamiltonians. *J. Chem. Phys.* 2012, **137**, 154114.
- [8] Li, Z.; Xiao, Y.; Liu, W. On the spin separation of algebraic two-component relativistic Hamiltonians: Molecular properties. *J. Chem. Phys.* 2014, **141**, 054111.
- [9] Lu, T.; Chen, F. W. Multiwfn: A multifunctional wavefunction analyzer. *J. Comput. Chem.* 2012, **33**, 580-592.
- [10] Hohenberg, P.; Kohn, W. Inhomogeneous Electron Gas. *Phys. Rev.* 1964, **136**, B864-B871.
- [11] Clark, S. J.; Segall, M. D.; Pickard, C. J.; Hasnip, P. J.; Probert, M. I. J.; Refson, K.; Payne, M. C. First principles methods using CASTEP. *Z. Krist.-Cryst. Mater.* 2005, **220**, 567-570.
- [12] Perdew, J. P.; Burke, K.; Ernzerhof, M. Generalized Gradient Approximation Made

- Simple. *Phys. Rev. Lett.* 1996, **77**, 3865-3868.
- [13] Tkatchenko, A.; Scheffler, M. Accurate Molecular Van Der Waals Interactions from Ground-State Electron Density and Free-Atom Reference Data. *Phys. Rev. Lett.* 2009, **102**, 073005.
- [14] Spackman, P. R.; Turner, M. J.; McKinnon, J. J.; Wolff, S. K.; Grimwood, D. J.; Jayatilaka, D.; Spackman, M. A. CrystalExplorer: a program for Hirshfeld surface analysis, visualization and quantitative analysis of molecular crystals. *J. Appl. Crystallogr.* 2021, **54**, 1006-1011.
- [15] Spackman, M. A.; Jayatilaka, D. Hirshfeld surface analysis. *CrystEngComm* 2009, **11**, 19-32.
- [16] Spackman, M. A.; McKinnon, J. J. Fingerprinting intermolecular interactions in molecular crystals. *CrystEngComm* 2002, **4**, 378-392.
- [17] Ma, H.; Lv, A.; Fu, L.; Wang, S.; An, Z.; Shi, H.; Huang, W. Room-Temperature Phosphorescence in Metal-Free Organic Materials. *Ann. Phys.* 2019, **531**, 1800482.
- [18] Hirata, S. Molecular physics of persistent room temperature phosphorescence and long-lived triplet excitons. *Appl. Phys. Rev.* 2022, **9**, 011304.
- [19] Herzberg, G.; Teller, E. Schwingungsstruktur der Elektronenübergänge bei mehratomigen Molekülen. *Z. Phys. Chem. (Leipzig)* 1933, **21B**, 410-446.
- [20] Albrecht, A. C. "Forbidden" Character in Allowed Electronic Transitions. *J. Chem. Phys.* 1960, **33**, 156-169.
- [21] Perrin, M. H.; Gouterman, M.; Perrin, C. L. Vibronic Coupling. VI. Vibronic Borrowing in Cyclic Polyenes and Porphyrin. *J. Chem. Phys.* 1969, **50**, 4137-4150.
- [22] Orlandi, G.; Siebrand, W. Mechanisms of vibronic intensity borrowing. *Chem. Phys. Lett.* 1972, **15**, 465-468.
- [23] Fulton, R. L. Vibronic Interactions. The Adiabatic Approximation. *J. Chem. Phys.* 1972, **56**, 1210-1218.
- [24] Rurack, K.; Spieles, M. Fluorescence quantum yields of a series of red and near-infrared dyes emitting at 600-1000 nm. *Anal. Chem.* 2011, **83**, 1232-1242.
- [25] Lakowicz, J. R. Principles of Fluorescence Spectroscopy; 3rd ed.; Springer, 2006.
- [26] Law, J.; Rennie, R. A Dictionary of Physics; 6th ed.; Oxford University Press, 2009.
- [27] Kleideiter, G.; Lechner, M. D.; Knoll, W. Pressure dependence of thickness and refractive index of thin PMMA-films investigated by surface plasmon and optical waveguide spectroscopy. *Macromol. Chem. Phys.* 1999, **200**, 1028-1033.